Observation of the Turnover between the Solvent Friction (Overdamped) and Tunneling (Nonadiabatic) Charge-Transfer Mechanisms for a Au/$Fe(CN)_6^{3-/4-}$ Electrode Process and Evidence for a Freezing Out of the Marcus Barrier

Dimitri E. Khoshtariya*,†,‡ and Tina D. Dolidze†

Institute of Inorganic Chemistry and Electrochemistry, Jikiya 7, Tbilisi 380086, and Institute of Molecular Biology and Biophysics, Georgian Academy of Sciences, Gotua 14, Tbilisi 380060, Georgian Republic

Leonid D. Zusman§,|| and David H. Waldeck*,§

Department of Chemistry, University of Pittsburgh, Pittsburgh, Pennsylvania 15260, and Institute of Inorganic Chemistry, Russian Academy of Sciences, Novosibirsk 630090, Russia

Received: November 8, 2000

By variation of the electronic coupling strength, the transition between the solvent-controlled regime (in which the electron-transfer rate constant depends on the solvent friction) and the nonadiabatic electron-transfer limit was observed for the Au/$Fe(CN)_6^{3-/4-}$ redox system. The solvent friction regime was demonstrated for a bare Au electrode by showing that the apparent standard rate constant was inversely proportional to the viscosity in water/glucose solutions containing 1 M KCl. The magnitude of the electronic coupling between the Au and the redox species was reduced by preparing *n*-alkanethiol-coated gold electrodes ($Au-S-(CH_2)_{n-1}-CH_3$ with $n = 2, 4, 6, 8$) of different thicknesses. For the case of a Au electrode coated by an ethanethiol monolayer ($n = 2$) the rate constant exhibited a fractional viscosity dependence, whereas the electrodes with $n = 4$, 6, and 8 methylenes in the film showed no viscosity dependence. This trend is indicative of an overall gradual turnover between the two regimes. In the nonadiabatic regime the distance dependence of the electronic coupling decay is 1.04 $Å^{-1}$, and its extrapolated value at the closest electrode−reactant distance is 3.5 kcal mol^{-1}. Analysis of the kinetic data, together with some results available in the literature, determines the intrinsic parameters of the charge-transfer step in both regimes. Corrections for the significant variation in the reactive site potential near the electrode (at the outer Helmholtz plane, OHP) and the reorganization free energy with the charge-transfer distance are taken into account. Evidence for a freezing out of the Marcus barrier (lowering by a factor of 2) was found for the process at the bare Au electrode, in accordance with theoretical prediction (Zusman, L. D. *Chem. Phys.* **1983**, *80*, 29).

1. Introduction

Because of their importance and fundamental nature great progress has been made in describing electron transfer reactions from the theoretical perspective. The charge transfer models were originally developed in two different limits: in the framework of the transition state (Eyring and others)[1] and the perturbation theory (Landau, Zener)[2] formalisms. These limits are also known as the adiabatic, or strong electronic coupling, regime[3,4] and the nonadiabatic, or weak electronic coupling, regime.[5−8] More recently, the adiabatic (short-range) electron-transfer mechanism was reconsidered in the spirit of a solvent friction theory[9] by several authors.[10,11] These more recent models[10,11] address the conditions for the experimental manifestation of the two extreme mechanisms, and of an intermediate regime between them. For heterogeneous electron transfer, substantial experimental evidence exists for the occurrence of the weak and strong coupling regimes. In contrast, little evidence is available that demonstrates the intermediate regime. This work provides experimental evidence for the transition between the strong and weak coupling limits in heterogeneous electron transfer for a given redox couple.

The weak electronic coupling (tunneling) mechanism has been demonstrated by using metal (Au, Hg)[12−16] or semiconductor (InP, e.g.)[17] electrodes that are derivatized with self-assembled monolayer films (SAM) of variable thickness. When the film is composed of alkane chains, a highly insulating barrier, which greatly reduces the electronic coupling between the electrode and the redox couple, is formed. The apparent heterogeneous rate constant k_{el} (usually corrected for double-layer effects and other factors arising from the system's inhomogeneity) is well described by an exponential behavior with respect to the electrode−reactant separation distance, R_e:[12−17]

$$k_{el} \propto \exp(-\beta R_e) \tag{1}$$

For saturated hydrocarbon spacers (SAMs), β values are typically found to have magnitudes of ~ 1 $Å^{-1}$. These observations can be considered as direct evidence for the tunneling (nonadiabatic) mechanism,[5−8] for which

$$k_{et} \propto (H_{if})^2 \tag{2}$$

and

* The corresponding authors. E-mail: Dimitri@biophys.acnet.ge, Dave@pitt.edu.
† Institute of Inorganic Chemistry and Electrochemistry.
‡ Institute of Molecular Biology and Biophysics.
§ University of Pittsburgh.
|| Deceased.

10.1021/jp0041095 CCC: $20.00
Published on Web 02/13/2001

$$H_{if} = H_{if}^0 \exp\left(-\frac{\beta}{2}R_e\right)$$

H_{if} is the electronic coupling matrix element, and H_{if}^0 is its value at the minimal donor−acceptor separation distance (vide infra).

The strong electronic coupling (solvent friction) mechanism has been demonstrated for many redox couples undergoing charge exchange at bare metal electrodes (e.g., Pt, Hg). The experimental signature of this limit is a rate constant that is viscosity dependent.[18−23] This dependence has been characterized by the power law form,

$$k_{el} \propto \eta^{-\gamma} \tag{3}$$

where η is the solution viscosity and γ is an "empirical" parameter. The experimental studies have changed the solvent viscosity in different ways, by the addition of inert viscous substances, by the variation of the solvent, or through the variation of applied pressure.[18−23] A viscosity dependence is considered to be evidence for the solvent friction (overdamped) mechanism, because the theoretical models[18−24] predict that the electron transfer rate constant is inversely proportional to the longitudinal dielectric relaxation time τ_L of the solvent (or $\tau_L^{-\gamma}$) and for simple Debye-type solvents $\eta \sim \tau_L$.[9−11,21] The parameter γ has a value in the range $0 < \gamma \leq 1$ (for the "full" solvent friction limit, $\gamma \rightarrow 1$).[8−10]

As suggested by recent theoretical models,[10,11,21] a turnover or intermediate regime between the two extreme mechanisms can be realized by the gradual variation of one, or several, characteristic parameters of the charge transfer process. Reports on the turnover between these regimes are extremely rare (e.g., see ref 24). For electron exchange processes, the turnover between the two mechanisms was first demonstrated by Weaver et al.[20] In that study a series of metallocene reactant species were used to change the strength of the electronic coupling parameter H_{if}. The present work uses a complementary approach to change the electronic coupling strength. By a gradual modification of the electrode surface with insulating layers of different thickness, it is possible to tune the electronic coupling strength but use the same redox couple. The Fe(CN)$_6^{3-/4-}$ redox couple was chosen for this study because the two different mechanisms were already observed at SAM-coated Au (tunneling)[13] and bare Pt (overdamped)[22a,c] electrodes. A new study was required because the different conditions in these experiments (different electrodes, different types and concentrations of supporting electrolytes) and the lack of data for the intermediate kinetic regime did not allow for a rigorous comparison. In the present work a rather smooth turnover between the strong and weak electronic coupling regimes (i.e., of overdamped and tunneling mechanisms) is found for the Fe(CN)$_6^{3-/4-}$ redox couple at a Au electrode in contact with an aqueous electrolyte solution. A gradual variation of the electrode−reactant distance, hence the electronic coupling, was achieved using the bare and the *n*-alkanethiol SAM (Au−S−(CH$_2$)$_{n-1}$−CH$_3$; n = 2, 4, 6, 8) coated electrodes. An analysis of the experimental results from the perspective of modern theoretical ideas allows for the determination of the characteristic parameters of the intrinsic charge-transfer step.

2. Is It a Proper Model System?

Kinetic data for nonadiabatic (tunneling) electron transfer have been collected for Au electrodes that are coated by alkanethiol or hydroxyalkanethiol monolayers with the number of methylene units in the range of n = 6−20.[13−15] For longer insulator chains, $n > 20$, the measured current becomes too low for accurate detection by conventional electrochemical techniques. The thinner SAMs ($n < 6$) were deemed less appropriate for kinetic studies because of certain disadvantages. Among them the following should be mentioned:

(a) Their performance is less reproducible than the longer chain SAMs. This variability has been ascribed to an increased tendency to form defects (pinholes, collapsed sites, etc.), as detected by the methods of optical ellipsometry and infrared external reflection spectroscopy.[12]

(b) The layers are permeable to common electrolyte anions (Cl^-, ClO_4^-, etc.) known to display specific adsorption at the metal electrodes.[12]

(c) Several physical factors/parameters, such as the double-layer correction and the medium reorganization energy, change dramatically at small distances from the electrode surface (i.e., the region from the bare surface to the thinnest alkanethiol-modified electrode), even if the solution composition is unchanged.

These effects complicate the theoretical analysis of the experimental data[12,14] and have led to the customary exclusion of kinetic studies at electrodes that are coated by short-chain modifiers.[13−16]

The redox reactions of the Fe(CN)$_6^{3-/4-}$ couple were extensively studied using bare Au and Pt electrodes,[25] in particular, with the aim of studying the solvent friction mechanism.[22a,c] On Pt electrodes the data displayed a clear Kramers-type ($\gamma \approx 1$) dependence on the solution viscosity, which was varied by using water/electrolyte/glucose solutions at high concentrations of supporting electrolyte (up to 1−2 M KCl, or LiCl) and glucose concentrations of 0−700 g L^{-1} (with relative viscosities η_r = 1−20).[22c] Hence, it was concluded that the Au(bare)/Fe(CN)$_6^{3-/4-}$ and the Au(−S−(CH$_2$)$_{n-1}$−CH$_3$)/Fe(CN)$_6^{3-/4-}$ (n = 2, 4, 6, 8) composites in 1 M KCl as a supporting electrolyte would be the most appropriate systems for probing the transition between the overdamped and the tunneling electron-transfer mechanisms.

The Au/Fe(CN)$_6^{3-/4-}$ was deemed the most appropriate for four primary reasons.

(a) The solvent friction mechanism was well-documented for a Pt(bare)/Fe(CN)$_6^{3-/4-}$ redox system[22c] and could be expected for a bare Au electrode under similar conditions.

(b) The alkanethiol SAMs on Au are the best characterized, highly ordered, and compact.[12−15] In addition, recent reports indicate that structural defects can be minimized by the increase of the *n*-alkanethiol adsorption time at the electrode (up to 24 h, and more).[15d]

(c) Accessibility of the SAM-coated Au surface by electrolyte anions, such as Cl^-, does not necessarily imply the existence of pinholes or other structural defects. The adsorption may take place through well-oriented SAM domains because of dynamic fluctuations in the SAM. The adsorption is driven by the specific interaction of the Au surface with the electrolyte anions. Recent results of Porter et al.[12a,c] indicate that small (and easily desolvated) ions can be readily adsorbed on a Au surface through the alkanethiol SAMs with $n < 10$, while larger (strongly solvated) ions, such as F(H$_2$O)$_x^-$ cannot (the latter is known also as a relatively poorly adsorbing ion on the bare metal surface).[26] As a result, the compact part of the double layer for the bare and the SAM-coated ($n < 10$) Au electrodes are more similar than previously thought.

(d) Recent work by Newton et al.[14a,b] provides an avenue for quantifying how the solvent reorganization energy depends on the electrode−reactant separation distance.

3. Experimental Section

Materials (Electrodes and Solutions). The working Au electrodes were either a rotating disk electrode (RDE), $d = 2$ mm (Radiometer, Copenhagen), or Au balls that were prepared by melting the end of a gold wire (99.99% purity) in a gas−oxygen flame. The diameter of the Au ball electrodes was ca. 2 mm. Both types were used as bare and SAM-modified electrodes, but the rotation procedure was applied only for the bare disk electrode. The RDE electrode was cleaned and polished with alumina powder (Buehler) on a Buehler polishing cloth through a series of 1.0, 0.3, and 0.05 μm grit sizes, followed by sonication in deionized water. The Au ball electrodes were cleaned by immersion in a hot Piranha solution (3:7, 30% H_2O_2 + concentrated H_2SO_4) for 5 s, followed by immersion in a room-temperature Piranha solution for 10 min, and subsequent rinsing with deionized water. The electrodes were coated with alkanethiols of different chain lengths ($HS-(CH_2)_{n-1}-CH_3$ ($n = 2-8$, Aldrich)) to create an insulating barrier above the Au surface. For this purpose both kinds of electrodes were cleaned by Piranha solution (as described above), rinsed with absolute ethanol and immediately transferred into the coating solution (*n*-alkanethiol solution, 2×10^{-3} M in ethanol) for 48 h or more, as recommended by Diao et al.[15d]

The solutions used in the voltammetry studies consisted of 2×10^{-3} M $K_3Fe(CN)_6$ and 1 M KCl in deionized water. The viscosity of the solutions was varied by the addition of anhydrous (+)-D-glucose (Aldrich). Glucose concentrations of 0, 200, 402, and 602 g/L were used and provided relative viscosity values of 1.002, 1.792, 3.953, and 11.245, respectively.[22c]

All other chemicals were of analytical grade and used as received.

Electrochemical Measurements. All voltammetric measurements were carried out on a PAR 273 potentiostat that was controlled with model 270 software (Princeton). A three-electrode configuration cell with a platinum wire auxiliary electrode and a silver/silver chloride (Ag/AgCl/saturated KCl) reference electrode was used throughout the studies. All potentials are reported with respect to this reference electrode. All the kinetic measurements were performed at a temperature of 24.5 ± 0.5 °C.

For the bare electrodes kinetic data were collected through two different experimental procedures, viz., the steady-state RDE and the cyclic voltammetry (CV) studies. In the case of the steady-state technique, the steady-state current I was measured as a function of the disk electrode's rotation speed ω, over the range from 500 to 4000 rpm. The value of the heterogeneous standard rate constant, k_{el}^0, was calculated through the expression[27a,b]

$$\frac{1}{I_\infty} = \frac{1}{mFSk_{el}^0 C_o} \tag{4}$$

where m is the number of transferred electrons (here $m = 1$), F is the Faraday constant, S is the electrode area, and C_o is the reactant's bulk concentration. I_∞ is a kinetic current that is determined from the intercept of the dependence of I^{-1} vs $\omega^{-1/2}$ at $\omega \rightarrow \infty$ and at the apparent standard potential of the redox couple, $E = E^0$. For the CV technique, the peak-to-peak separation between the anodic and cathodic waves (ΔV_p) was measured at different scan rates (υ). Values of the standard rate constants were determined from a numerically evaluated relationship between ΔV_p and the function Ψ, given by equation derived by Nicholson:[28]

$$\Psi = \frac{(D_O/D_R)^{\alpha/2}(RT)^{1/2}k_{el}^0}{(\pi m F D_O \upsilon)^{1/2}} \tag{5}$$

where α is the transfer coefficient, R is the gas constant, T is the absolute temperature, D_O and D_R are the diffusion coefficients of the reactant's oxidized and reduced forms, $Fe(CN)_6^{3-}$ and $Fe(CN)_6^{4-}$, respectively. For the bare electrodes the two approaches gave consistent rate constants.

The resistance of an electrochemical cell should increase to some extent with solvent viscosity, and it is important to determine whether this phenomenon contributes to the observed viscosity effect. Using a typical value for the uncompensated resistance,[27c] one finds that the uncompensated resistance is less than 1% of the actual faradaic resistance at the bare electrode in the absence of glucose. Although the uncompensated resistance increases with viscosity, so does the faradaic resistance (resulting from the dynamical effect on the electron transfer rate), and the contribution is not likely to change much from 1%. This conclusion was corroborated by experiment. No change (outside of experimental error) was found for the electron-transfer rates found on bare Au electrodes in which the area differed by as much as four times (disk and balls, respectively) and for solutions with different reactant concentrations in the range 5×10^{-4} to 5×10^{-3} M. Hence the uncompensated cell resistance plays a minor role in our experiments.

Another important methodological aspect (chemisorption of the reactant on the bare Au electrodes) is connected to an important theoretical aspect (the problem of the reactants' distance from the electrode surface during electron transfer) (vide infra). Previous studies show that direct adsorption of hexacyanoferrate ions at the Au or Pt surface leads to the immediate decomposition of the species and the irreversible blockage of the electrode surface by the decomposition products (see refs 22c and 25f and literature cited therein). Rigorous cleaning of the working electrode before each measurement and careful instrumental control[22c,25f] eliminated this side effect. The success of the methodology could be verified by the reversibility of the voltammograms. For this reason we conclude that contact between the redox species and the electrode does not contribute significantly to our data.

The rate constants for the SAM-coated electrodes were determined using the steady-state voltammetry method, because the ($n = 4, 6, 8$) SAM-coated electrodes were not mechanically stable enough to reliably withstand the electrode rotation. For the voltammetric data, the kinetics was accessed from the initial portions of steady-state voltammograms, where the mass transport effect (and other effects leading to the nonlinearity of the dependence of $\log(k_{el})$ versus $\Delta E = E - E^0$, known as Tafel plots) on the measured current is negligible (see ref 13a).

The capacitance of the bare and *n*-alkanethiol-coated Au electrodes were determined through the cyclic voltammograms of blank electrolyte solutions (charging currents), as recommended in ref 12c, in the "double-layer" region (around $E \sim 0$ and scan speed of $\upsilon = 100$ mV s^{-1}).

4. Results

Kinetic Effect of *n*-Alkanethiol SAMs. Cyclic voltammetry (CV) was used to obtain kinetic and capacitance data for the SAM-coated electrodes and to assess the quality of the films, i.e., the defects and their development in time.[12-14] Figure 1 presents CV curves (recorded at $\upsilon = 100$ mV s^{-1}) for Au electrodes that are coated with alkanethiols having methylene unit numbers of $n = 2$, 4, and 8. Data for the bare Au, and the

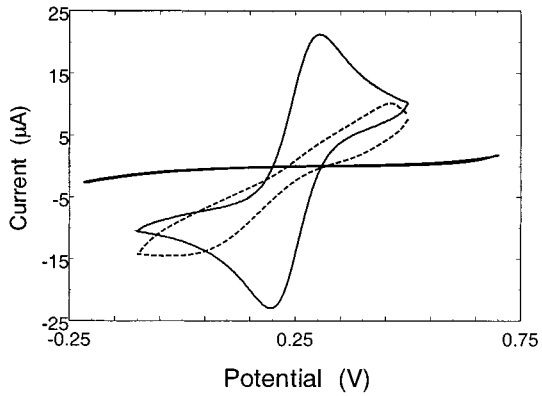

Figure 1. Cyclic voltammograms for the *n*-alkanethiol SAM-coated Au electrodes. Peaked curve: $n = 2$. Flat curve: $n = 8$. Intermediate curve (dashed line): $n = 4$. Scan rate: 0.1 V s^{-1}.

methylene unit number $n = 6$ are omitted for clarity. The dramatic change in the measured current density (the measured rate constants) and the shape of CV curves with the increase in the methylene number, *n*, indicates an increased hindrance to electron transfer. This observation is in general agreement with earlier data on SAM-coated electrodes with longer chains in which it was interpreted as a manifestation of the tunneling mechanism.[13−16] Table 1 presents the values of experimental (apparent uncorrected) standard rate constants, the corresponding nonadiabatic rate constants, the intrinsic charge transfer (corrected) rate constants, the double-layer capacitance, and some calculated parameters (all in the absence of viscous additives).

The role of pinholes, collapsed sites, and other possible defects (except a pronounced transparency to Cl^- ions, see below) can be considered as negligible for the following reasons:

(a) All the current−potential curves, in all instrumental regimes applied, were well-behaved and repeatedly reproducibly for 20−30 min, before the first distortions from SAM defects appeared.

(b) For the case of the shortest alkanethiol chain (viz., $n = 2$), the CV curves were peak-shaped as in the case of the bare electrode. No sigmoidal curves, which are indicative of kinetically active pinhole-like defects,[12c] were observed in this case (except for a few cases that were rejected).

(c) For SAMs with *n* equal to 6 and 8, no peak-shaped curves, which could be indicative of a large contribution from defect sites,[15d] were observed (except for a few rejected cases).

For these reasons the electrochemical data were determined to be reliable. The heterogeneous standard rate constants were determined as a function of solvent viscosity and the SAM film thickness.

Kinetic Viscosity Effects. Figure 2 shows the dependence of the apparent standard rate constant for electron exchange between the Fe(CN)$_6^{3-/4-}$ redox couple and the Au electrodes (bare and *n*-alkanethiol-coated (Au−S−(CH$_2$)$_{n-1}$−CH$_3$; $n = 2$, 4, 6, 8)) as a function of the solution viscosity. The results of both experimental techniques, steady-state RDE (top, filled circles and solid line) and CV peak-separation (top, open diamonds and dashed line), are presented for the bare electrode. The RDE technique yielded precise kinetic data with an experimental error of less than 5%. The rate constant that was obtained for the bare electrode through the RDE technique was corrected for a roughness factor of 2.3, as determined in previous work[25d] under similar polishing conditions. The values of the rate constants that were obtained from the CV peak separation data usually had a somewhat larger experimental error.[28] For this reason, voltammograms were collected for each gold ball electrode at 3−4 different scan rates in order to improve the statistics. The values reported in Table 1 are the average rate constants obtained from 4−6 different electrodes, each of which are in turn the average of 3−4 measurements at different scan rates. The CV peak separation method, in contrast to the steady-state technique (including RDE studies), does not require determination of the electrode area, but rather the reactant's diffusion coefficient. The diffusion coefficient for the present redox couple, at the various concentrations of glucose used here, were determined previously.[22c]

From Figure 2 it is evident that rate constant data obtained from the two different methods give similar results for the bare Au electrode. This fact points to the reliability of the less precise CV peak separation technique for the cases where the more precise RDE technique could not be implemented (e.g., for the case of an alkanethiol SAM with a methylene unit number $n = 2$, vide infra). For the bare Au electrode the kinetic data display a "full" Kramers-type dependence of the apparent standard rate constant on the solution viscosity with a slope of $\gamma = 0.96 \pm 0.04$; see eq 3. This result is very similar to one obtained earlier for a Pt(bare)/Fe(CN)$_6^{3-/4-}$ redox system under the same experimental conditions (the same electrolyte and viscous additive). This observation indicates that both the bare Pt and Au electrodes operate in the strong coupling, or adiabatic, limit.

For the SAM-coated Au electrodes, the dependence of the apparent standard rate constant on the solution viscosity was studied by the cyclic voltammetry method. For the ethanethiol SAMs it was possible to use the peak separation method to extract the electron transfer rate constant. Despite some scatter, the data for the ethanethiol-coated electrode clearly indicate a fractional viscosity effect, with a slope of $\gamma \approx 0.3$ (Figure 2). For the thicker SAMs ($n = 4$, 6, 8) the rate data were found from the exponential region of the current−voltage curves. Because the initial portions of voltammograms that were free of mass transport effects were small, up to 6 gold ball electrodes were used with the aim of statistical improvement of the data. The accuracy of this method increases while going from short to longer alkanethiol chains because the extent of the voltammogram that is free of mass transport limitations ("Tafel-like" regions) becomes larger at $n = 6$, 8. The results obtained for $n = 4$, 6, 8 clearly indicate an absence of the viscosity dependence and the establishment of a tunneling mechanism (Figure 2). This behavior is evident in Figure 3, in which all the experimental data for the apparent standard rate constants are plotted versus the methylene unit number, *n*. Even without including the distance-dependent corrections discussed below, it is evident that a turnover between the solvent friction and tunneling regimes occurs for the ethanethiol SAMS (i.e., the thinnest SAM, corresponding to an electrode−reactant (center) separation distance of ca. 8.5 Å).

5. Discussion

General Considerations. To quantify the dependence of the kinetics on the system's parameters, the "encounter-preequilibrium" formalism is convenient.[29] This approach treats the experimentally determined heterogeneous or bimolecular apparent rate constant as an integral over the product of the statistical distribution of reactant configurations and the "local" (or unimolecular) rate constant at each configuration. In general, this integral includes variations in the major intrinsic parameters of the charge-transfer step and could be quite complex for an inhomogeneous system. For systems of the type studied here, however, the spatial range of reaction sites that contribute to the apparent heterogeneous standard rate constant, k_{el}^0, is

TABLE 1: Experimental and Calculated Values of Different Kinetic and Intrinsic Energetic Parameters for the Electron Exchange Involving the Au(bare)/Fe(CN)$_6^{3-/4-}$ and Au(−S−(CH$_2$)$_{n-1}$−CH$_3$)/Fe(CN)$_6^{3-/4-}$ (n = 2, 4, 6, 8) Redox Systems (Calculated Values in Italics)

no.	type of electrode, mechanism	R_e, Å	$\ln(k_{el}^0)$, cm s^{-1}	ΔG_r^*, kcal mol^{-1}	H_{if}, kcal mol^{-1}	ΔG_a^*, kcal mol^{-1}	$-\Phi_r$, V	$\ln(k_{el(NA)}^0)$, cm s^{-1}	$-\ln(K_A)$, cm	$\ln(k_{et}^0)$, s^{-1}	C, μF cm^{-2}
1	bare (n = 0) SF (obsd	*7.9*	−3.30	8.0	*~1*	*≈1*	0.125		*28.10*	*24.80*	35
2	bare (n = 0) NA (hypoth)	*4.3*	*1.46*	*15.9*	*3.5*	*≈0.5*	0.125	*1.46*	*28.10*	*29.55*	35
3	bare (n = 0) NA (hypoth)	*7.9*	*−2.60*	*19.6*	*~1*	*3.9*	0.125	*−5.80*	*28.10*	*25.50*	35
4	SAM (n = 2) med (obsd)	*8.5*	−5.60	*19.9*	*0.40*	*4.6*	*0.065*	*−5.38*	*23.44*	*17.84*	33
5	SAM (n = 4) NA (obsd)	*10.7*	−7.40	*21.0*	*0.13*	*5.1*	*0.051*	−7.40	*22.40*	*15.00*	30
6	SAM (n = 6) NA (obsd)	*12.9*	−9.60	*21.6*	*0.040*	*5.4*	*0.043*	−9.60	*21.74*	*12.14*	25
7	SAM (n = 8) NA (obsd)	*15.2*	−12.0	*22.1*	*0.012*	*5.5*	*0.037*	−12.0	*21.28*	*9.30*	16

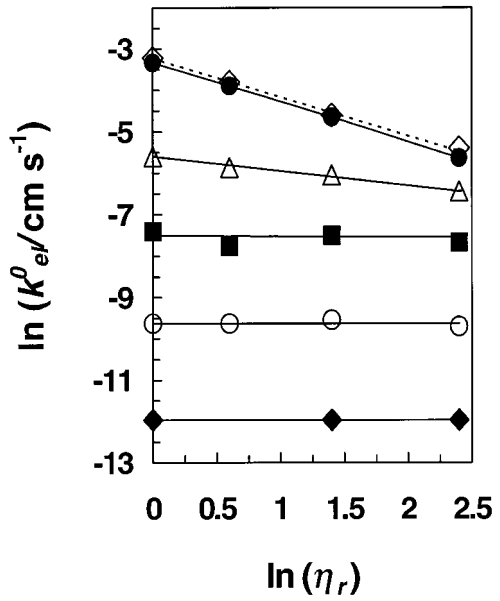

Figure 2. Viscosity dependence of the electron-transfer rate constant for the bare Au/Fe(CN)$_6^{3-/4-}$ (filled circles, RDE method; open diamonds, CV method) and SAM-coated electrodes (Au[−S−(CH$_2$)$_{n-1}$−CH$_3$]/Fe(CN)$_6^{3-/4-}$ with n = 2 (open triangles), n = 4 (filled squares), n = 6 (open circles), n = 8 (filled diamonds)).

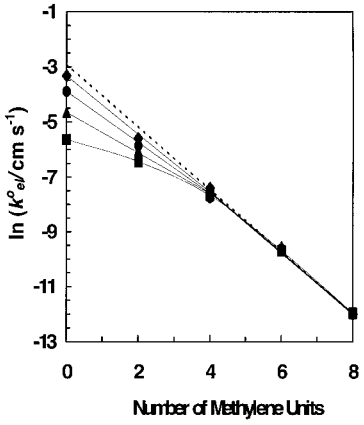

Figure 3. Logarithm of the experimental standard rate constant plotted against the number of methylene units at different relative viscosities η_r (η_r = 1, diamonds (CV method); η_r = 1.8, circles; η_r = 4.0, triangles; η_r = 11.25, squares. The dashed line shows a linear extrapolation for the distance dependence of the n = 4, 6, and 8 rate constant data.

expected to be quite narrow.[20,29] In this limit, the integral may be replaced by the product

$$k_{el}^0 = K_A k_{et}^0 \tag{6}$$

in which K_A is the "equilibrium constant" and k_{el}^0 is the intrinsic rate constant. K_A is defined as

$$K_A = \delta R_e \exp\left(\frac{-Z_{eff} F \Phi_r}{RT}\right) \tag{7}$$

and describes the concentration profile of the reactant near the electrode surface. In this expression δR_e is the "effective thickness" of the reaction zone (expected to be of the order of angstroms).[29] Its size reflects the spatial extent over which most of the electron transfer occurs (i.e., the part of the space integral over which the intrinsic charge-transfer constant (k_{et}^0) makes the major contribution to the current). Because of the exponential decay of the rate constant with distance (see Figure 3), this region is quite narrow. Z_{eff} is the effective charge of a reactant ion and Φ_r is the effective potential at the average distance of the electron transfer, usually near the outer Helmholtz plane (OHP).[29] The superscript "0" on k_{el}^0 and k_{et}^0 specifies the standard heterogeneous rate constant that is determined at the formal potential of the redox couple ($E = E^0$) and corresponds to a free energy change of zero, $\Delta G_o^* = 0$. The form of the intrinsic rate constant k_{et}^0 will depend on the regime, adiabatic or nonadiabatic, for the electron-transfer mechanism.

In the adiabatic, or solvent-controlled, regime the intrinsic (unimolecular) rate constant has been written as[10a,18,19,22c,23]

$$k_{et(SF)}^0 = \nu_{eff}\left(\frac{\Delta G_r^*}{16\pi RT}\right)^{1/2} \exp\left(-\frac{\Delta G_a^*}{16\pi RT}\right) \tag{8}$$

where ν_{eff} is a characteristic frequency for the relaxation of solvent molecules or solvent/solute clusters, ΔG_r^* is the reorganization energy, and ΔG_a^* is the activation free energy. It has been common to use a dielectric continuum approximation to obtain ν_{eff}. For a Debye-type solvent, one[21] finds that

$$\nu_{eff} = \nu_L = \tau_L^{-1} = \left(\frac{\epsilon_s}{\epsilon_\infty}\right)\frac{RT}{3\eta V_m} \tag{9}$$

where τ_L is the longitudinal relaxation time of the solvent polarization, which is proportional to the Debye relaxation time and, thus, to the solvent (solution) viscosity, η.[30] The other parameters in eq 9 are the molar volume V_m, the static dielectric constant ϵ_S, and the high-frequency dielectric constant ϵ_∞. More recent and precise theoretical treatment provides a somewhat different expression:[10b,c,d,f]

$$k_{et(SF)}^0 = \nu_{eff}\left(\frac{\Delta G_r^*}{\pi^3 RT}\right)^{1/2} \exp\left(-\frac{\Delta G_a^*}{RT}\right) \tag{10}$$

Under the present conditions this result differs from eq 9 by only a factor of about 1.6. An additional logarithmic term that appears in the original expression,[10c,d,f] is omitted here because its contribution was found to be negligible.[29]

In the nonadiabatic (or weak coupling) regime, the classical expression for the intrinsic rate constant is written as[5−8]

$$k^0_{et(NA)} = \frac{(H_{if})^2}{\hbar}\left(\frac{\pi}{RT\Delta G^*_r}\right)^{1/2} \exp\left(-\frac{\Delta G^*_a}{RT}\right) \qquad (11)$$

For heterogeneous electron transfer this expression takes a somewhat different form[10c,f]

$$k^0_{et(NA)} = \frac{(H_{if})^2}{\hbar}\rho_m\left(\frac{\pi^3 RT}{\Delta G^*_r}\right)^{1/2} \exp\left(-\frac{\Delta G^*_a}{RT}\right) \qquad (12)$$

where ρ_m is the density of electronic states in the metal (electrode). It is commonly accepted in the literature that the two parameters, ΔG^*_r and ΔG^*_a, appearing in eqs 8 and 10−12 are connected through the simple relationship, $\Delta G^*_a \approx {}^1/_4\Delta G^*_r$. The exact expression[3,5,8] behind this formula is

$$\Delta G^*_a = \frac{(\Delta G^*_r - \Delta G^*_o)^2}{4\Delta G^*_r} - H_{if} \qquad (13)$$

Equation 13 indicates that when the values of ΔG^*_r and H_{if} are comparable and ΔG^*_o is zero, a simple "one-fourth" rule is no longer valid. In the nonadiabatic limit H_{if} is usually small compared to ΔG^*_r and the one-fourth rule applies.

Rate Constant for Bare Au. It is useful to begin the calculation of the rate constant for the simple case of the bare Au electrode, which lies in the solvent-controlled regime. First, the values of the activation free energy and the effective frequency in eqs 8−10 will be estimated. With these values in hand it is possible to calculate the intrinsic electron-transfer rate constant through eq 10. A comparison of this intrinsic rate constant with the standard apparent rate constant is then used to determine K_A, by eq 6.

The values of the intrinsic energy parameters, ΔG^*_a and ΔG^*_r, can be determined in two different ways.

(a) From studies of the temperature dependence (from 0 to 60° C) of the standard apparent heterogeneous rate constants k^0_{el}, [25c] it was demonstrated that the apparent enthalpy of activation, $\Delta H^{\#}$, was equal to 4.8 ± 0.2 kcal/mol and was relatively constant for a wide range of solution conditions (0.1−1.0 M KCl and 0.5−4.5 M $LiNO_3$). At the same time, the apparent standard rate constant displayed a strong dependence on the nature and concentration of the electrolyte's cationic component.[25b,c,f] Hence, the variation of k^0_{el} within the series has a purely entropic origin and can be associated with changes of the preequilibrium term, eq 7 (vide infra). In this case, the experimental enthalpy of activation can be considered as the sum of the intrinsic enthalpy of activation and the enthalpy of activation for the solvent's polarization relaxation time (which is taken as that for the viscosity ΔH_η, see eq 9), so that

$$\Delta H^{\#} = \Delta H_\eta + \Delta H^*_a \qquad (14)$$

Assuming that the reorganization entropy is negligible[5c,d,8a,b,c] and using eq 13, it is possible to write the free energy of activation as the enthalpy of activation

$$\Delta G^*_a \approx \Delta H^*_a = \Delta H^{\#} - \Delta H_\eta \qquad (15)$$

Over the temperature range of 0−60° C, the solution's viscosity is well-described by[31]

$$\eta = \eta_o \exp(\Delta H_\eta/RT) \qquad (16)$$

where the parameters η_o and ΔH_η are considered to be temperature independent. From the published data[31] the value of ΔH_η for pure water is determined to be 3.7 ± 0.2 kcal mol^{-1}. Accepting this value for the standard case (without viscous additive) and using eq 15, one finds $\Delta G^*_a \approx 4.8-3.7 = 1.1 \pm 0.4$ kcal mol^{-1}. If H_{if} is taken to be 1 kcal mol^{-1} (as is justified below), then eq 13 gives a ΔG^*_r of 8.0 ± 1.2 kcal mol^{-1}, an unexpectedly low value (vide infra).

(b) Another way to obtain ΔG^*_a and ΔG^*_r is from curved Tafel plots (plots of log(k_{el}) vs the applied overpotential, ΔE, corrected for the mass transport effects).[13e,25d] The value of ΔG^*_r can be directly estimated from the transfer coefficient α (determined from the slope of the Tafel plot) by assuming that the preequilibrium constant (eq 7), which is determined by the effective potential Φ_r, is rather insensitive to electrode potential changes. The transfer coefficient changes with the overpotential, from a value of 0.5 (a customary value at the zero overpotential) to 1 or 0, according to eq 17:[3,5,8]

$$\alpha = \frac{\partial(\Delta G^*_a)}{\partial(\Delta G^*_o)} = 0.5 + \frac{\Delta G^*_o}{2\Delta G^*_r} = 0.5 - \frac{mF\Delta E}{2\Delta G^*_r} \qquad (17)$$

Tafel plots for the Au(bare)/Fe(CN)$_6^{3-/4-}$ in 1 M KF and Pt(I-coated)/Fe(CN)$_6^{3-/4-}$, in 1 M KCl were obtained in previous work.[25d,e] In each case the value obtained for ΔG^*_r from eq 17 is 8.0 ± 1.0 kcal mol^{-1}. The agreement between the three determinations of ΔG^*_r using two different procedures is considered to be excellent. However, the magnitude of ΔG^*_r is too small when compared to that expected on the basis of simple calculations or the comparison with related ones from homogeneous electron-transfer studies.

It is also possible to estimate a value for ν_{eff} in the context of a dielectric continuum model. A number of considerations validate the use of such a simple treatment for the solution's polarization response. Pure water exhibits at least two characteristic relaxation times, 8−9 ps and 1−2 ps, at room temperature.[30] It has been suggested that the longer time be ascribed to hindered displacement and the shorter time to hindered rotation of the water molecules.[30b] Although it is not a simple Debye-type solvent, it is reasonable to take the slower relaxation[10d,f] since it makes the largest contribution to the dielectric loss. At first glance, the composition of the reactant's environment at the active site near the electrode would appear to be very different from pure water, especially in the presence of the viscous additive, glucose. Nevertheless, it was concluded recently (based on studies of the viscosity effect on the reactant's diffusion coefficient)[22c] that the preferential solvation of Fe(CN)$_6^{3-/4-}$ reactant species by water molecules is similar in pure water and water/electrolyte/glucose mixtures.[22c] At the same time, the linear relationship between the ln(k^0_{el}) and ln(η_r) for bare Pt[22c] and Au (present work, Figure 2) electrodes strongly suggests that the Debye−Stokes−Einstein dependence, eq 9, is applicable. In addition, the dependence of the first solvation shell's dynamics on the redox state of the hexacyanoferratte species was demonstrated by the method of difference O−D overtone spectroscopy of heavy water as a solvent.[32] It seems that the addition of glucose does not displace the first solvation shell of the water but affects its dynamics through the common hydrogen-bonded network.[22c] A value of $\epsilon_s^W \sim 20$ is used for the diffuse part of the double layer near the OHP at the bulk concentration of 1 M KCl.[30d] This value, together with the

Debye relaxation time of $\tau_D = 8.5$ ps, yields $\nu_{eff} = \nu_L = (\epsilon_S/\epsilon_\infty)\tau_D^{-1} = 4.7 \times 10^{11}$ s^{-1} (estimated for $\epsilon_S = 20$ and $\epsilon_\infty = 5$). The latter value is somewhat different from that accepted for pure water (1.9×10^{12} s^{-1} at $\epsilon_S = 78$).[20,21] Some variation of this parameter over a reasonable range does not effect the conclusions.

Using these values for the parameters in eqs 6 and 8, it is possible to estimate the intrinsic rate constant and K_A. Using ΔG_a^* of 1.1 kcal/mol, ΔG_r^* of 8.0 kcal/mol, and ν_{eff} of 4.7×10^{11} s^{-1} in eq 8 gives an intrinsic rate constant k_{et}^0 of 5.0×10^{10} s^{-1} at 300 K. Combining this value with the experimental value of the apparent standard rate constant for a bare electrode, $k_{el}^0 = 0.037$ cm s^{-1}, and using eq 6, one finds a value for K_A of 7.5×10^{-13} cm, which seems to be rather low. In large part, the small value of K_A can be rationalized as a double-layer effect (see below).

The Double Layer. Previous work has argued that for K^+ (and other alkali ions) as the cation of the supporting electrolyte (at concentrations above ca. 0.1 M), the predominant redox-active species are $[K_2Fe^{II}(CN)_6]^{2-}$ and $[KFe^{III}(CN)_6]^{2-}$, corresponding to $Z_{eff} = -2$.[22c,25f] These species arise from asymmetrical contact-type ion association and should be distinguished from more traditional (Gouy−Chapman−Stern) double-layer effects. A detailed discussion of the role played by these electrolyte cations is provided elsewhere.[32b] It is well established that the formal potential of the $Fe(CN)_6^{3-/4-}$ redox couple, is 200−300 mV more positive than the potential of zero charge for the Au electrode.[26] Hence, a favorable Coulomb interaction between the positively charged electrode and the negatively charged reactant ions might be expected. In contrast, the calculated value of K_A is very low, indicative of a repulsive interaction between the electrode and the redox couple. K_A increases linearly with the increase of electrolyte concentration (as follows from the increase of the apparent heterogeneous rate constant, k_{el}^0), and displays sensitivity to the nature of the electrolyte's cationic component.[25] This behavior indicates a strong inhibiting effect by the compact part of the double layer consisting of adsorbed electrolyte anions, and a catalytic effect of electrolyte cations situated in the diffusive part of the double layer.[22c] Moreover, the effect of different anions is rather similar, whereas that of different cations varies significantly. This behavior is consistent with the participation of desolvated anions in the compact part of the double layer, and mostly solvated cations (except those stoichiometrically associated with the hexacyanoferrate reactant ions) in the diffusive part. Scheme 1 illustrates this view of the interfacial region. Using values of $Z_{eff} = -2$ and $\delta R_e \approx 10^{-8}$ cm (ca. 1 Å), eq 7 gives a Φ_r value of −125 mV. This value of Φ_r is quite reasonable for the OHP in the presence of specifically adsorbed Cl^- and corresponds to a change in the sign of Φ within the compact part (see refs 26 and 33). According to the Gouy−Chapman−Stern model,[33] the corresponding effective charge density (σ_{eff}) is given by

$$\sigma_{eff} = \sigma_{Cl^-} - \sigma_M = (8RT\epsilon_o\epsilon_S C_o)^{1/2} \sinh\left(\frac{zF\Phi_r}{2RT}\right) \quad (18)$$

where z is the charge on the electrolyte's cationic component (forming the diffuse part of the double layer) and $\sigma_{Cl}-$ and σ_M are the charge density arising from the specifically adsorbed chloride ions and the metal surface, respectively (in this case, $|\sigma_{Cl}-| \gg |\sigma_M|$). If $C_o = 1$ M and $\epsilon_S = 20$, then σ_{eff} is found to be ca. 30 μC cm^{-2}. The estimated value for the Cl^- coverage on the electrode lies in the range of $\theta \sim 0.25-0.30$, a value that is consistent with the overall description.[34] Note that the effect of glucose on Φ and Φ_r is considered to be negligible. This assumption is corroborated for a Hg electrode, where the Φ_r changed by less than 4 mV upon the addition of a large amount of sugar (48% by mass).[22b]

SCHEME 1: Interfacial Region Envisioned for the Bare Electrode (Rectangle)[a]

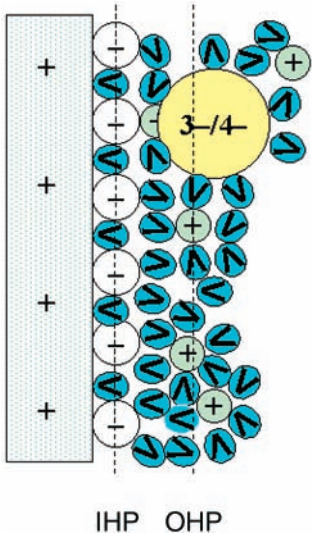

[a] The circles with the minus sign represent Cl^-, the circles with the plus sign represent K^+, the $Fe(CN)_6^{3-/4-}$ species are represented by a circle with "3−/4−" label, and the water solvent is illustrated by a circle with a "**V**" symbol. The inner Helmholtz plane (IHP) and the outer Helmholtz plane (OHP) are indicated by the vertical dashed lines.

Because of its large impact on K_A, it is important to consider possible changes in Φ_r when going from the bare Au to SAM-coated electrodes. As discussed earlier, literature data indicate that electrolyte anions, such as Cl^-, may penetrate through *n*-alkanethiol SAMs with $n = 2-8$ and form a compact part of the double layer that is similar to the bare Au case. This effect can be detected by capacitance measurements as described in the Experimental Section (section 3). Deviation of the SAM-coated electrode's capacitance from the general linear dependence of $1/C$ vs n (where C is the double-layer capacitance) was detected for chain lengths with $n = 2-6$.[12a,c] For short chain lengths the C values approach those reported for a bare Au electrode ($C \sim 30-40$ μF cm^{-2}).[25c] The analogous experiments performed in the present work revealed similar behavior (see Figure 4). It is clear from Figure 4, that the double-layer capacitance of SAM-coated Au electrodes at $n = 2$, 4, 6 was similar to that of the bare Au electrode, and only at $n = 8$ is a change evident (increase of $1/C$). As the experimentally determined double-layer capacitance is largely determined by the compact part,[33] this result is consistent with the earlier finding that thinner SAMs are transparent with respect to easily desolvated anions that are capable of specific adsorption on the Au surface. However, larger ionic aggregates, such as redox active $[K_2Fe^{II}(CN)_6]^{2-}$ and $[KFe^{III}(CN)_6]^{2-}$ species, or solvated counterions forming the diffuse part of the double layer, $[K(H_2O)_x]^+$, cannot move through the SAMs, because of either steric and/or thermodynamic reasons (e.g., the K^+ ion cannot be stabilized at the positively charged SAM-coated Au surface, nor inside the hydrophobic SAM interior). Consequently, for the systems in this study, the diffuse part of the double layer (OHP) will be separated from the compact part (IHP) by the alkanethiol spacer, which itself is free of charge. Scheme 2 illustrates this description of the interface.

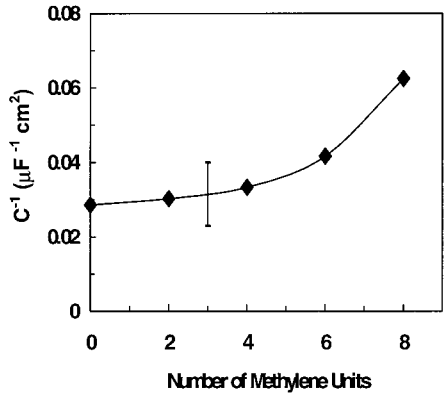

Figure 4. Reciprocal of the experimentally determined capacitance of the bare and SAM-coated Au electrodes plotted versus the number of methylene units. The diamonds are experimental points, and the curve is drawn as a guide to the eye. The error is indicated by the bar at $n = 3$.

SCHEME 2: Interfacial Region Envisioned for the SAM-Coated Electrode[a]

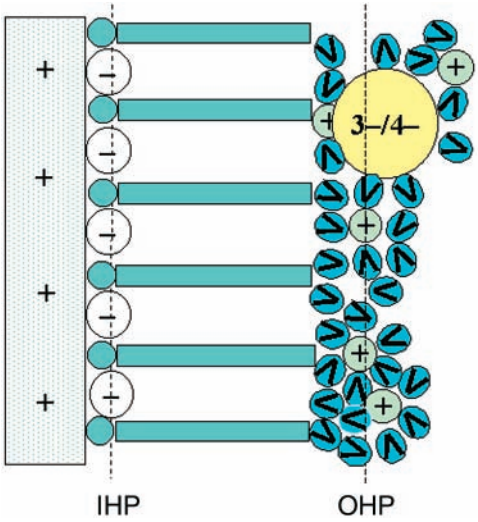

[a] The symbols have the same meaning as in Scheme 1. The plain circles are S atoms that are covalently linked to the Au electrode and the alkane chains (represented by horizontal rectangles).

This view of the interfacial region provides a self-consistent explanation for the capacitance data and Φ_r. Assuming that the chloride coverage does not change significantly, one can conclude that the potential next to the IHP (crossing the layer of specifically adsorbed chloride ions) should be essentially the same through the range of systems investigated, including processes at the bare and SAM-coated Au electrodes. This assumption is justified by the behavior of the capacitance data.[35] The potential at the OHP should be different, however. In the case of a bare electrode, the potential drop in the direction of the bulk solvent can be approximately described by the exponential function[33]

$$\Phi_r = \Phi_r^0 \exp(-\lambda R_e) \tag{19}$$

where Φ_r^0 is the maximum negative potential next to the IHP and $1/\lambda$ is the characteristic thickness of the diffuse layer in the absence of SAM films (i.e., formed by the electrolyte). Figure 5 (thin curve) shows the potential as a function of the electrode−reactant separation distance, according to eq 19 with a characteristic value of $\lambda = 0.33$ Å^{-1}, which is typical for 1 M electrolytes.[33] The function was normalized to have a value of

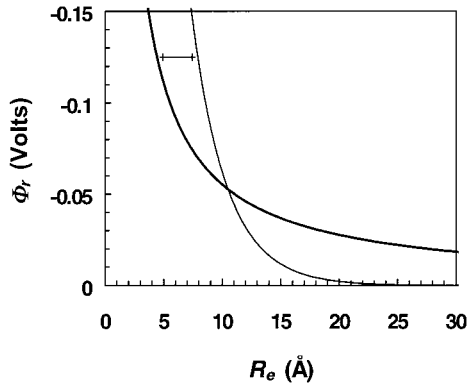

Figure 5. Thick curve giving the value of the Φ_r potential at the OHP for the *n*-alkanethiol-coated electrodes (according to eq 20). These values were used for the rate constant corrections given in Figure 7. For illustrative purposes, the calculated Φ_r potential is shown as a function of the electrode−reactant separation distance for the bare electrode (thin line). The horizontal bar indicates the distance shift corresponding to the Cl^- diameter (see text for more details).

−0.125 V at the electrode−reactant separation of 7.9 Å. The value of 7.9 Å is obtained from the diameter of a chloride ion (3.6 Å) and the radius of the redox couple (4.3 Å). Equation 19 is valid for a potential drop within the diffuse layer, but not inside the insulating SAM films.[34] For the SAM case the following expression can be employed:

$$\Phi_r = \frac{1}{4\pi\epsilon_0\epsilon_S R_e}\int_S \sigma_{eff}\, dS \tag{20}$$

where σ_{eff} is the effective charge density at the IHP, and S is the electrode's effective area. Figure 5 (bold curve) shows the value of the potential at the OHP as a function of the electrode−reactant separation according to eq 20. The potential function was normalized to have a value of −0.125 V at the distance of 4.3 Å (close contact). This normalization was chosen because specifically adsorbed Cl^- generate nearly the same IHP (as indicated by the capacitance data) as the bare Au, but the electrode−reactant spacing is controlled by the width of the SAM. In other words, for the SAM-coated electrodes the electrode−reactant separation distance does not include the Cl^- ion diameter. The OHP potentials corresponding to SAMs with $n = 2$, 4, 6, and 8 at the estimated separation distances of 8.5, 10.7, 12.9, and 15.2 Å, respectively (according to ref 14a), and the corresponding values of the preequilibrium constants are listed in Table 1.

Reorganization Free Energy. A quantitative understanding of the reaction kinetics requires a determination of changes in the intrinsic (Marcus-type) reorganization free energy, ΔG_r^*, which determines the intrinsic (viscosity independent) activation free energy (see eq 13). The original Marcus model provides simple expressions for the reorganization energy.[3,8] In particular, the reorganization energy ΔG_r^* is divided into an inner sphere free energy $\Delta G_{r(IS)}^*$ and an outer sphere reorganization energy $\Delta G_{r(OS)}^*$, so that

$$\Delta G_r^* = \Delta G_{r(IS)}^* + \Delta G_{r(OS)}^* \tag{21}$$

The inner sphere reorganization energy is determined by the internal modes of the redox system. For Fe(CN)$_6^{3-/4-}$ it is taken to be 1.4 ± 0.2 kcal/mol.[13e,22c] An expression for the outer sphere reorganization energy is obtained by approximating the redox couple as a spherical cavity that is immersed in a dielectric continuum, such that

$$\Delta G^*_{r(OS)} = \frac{(\Delta e)^2 N_A}{4\pi\epsilon_o}\left(\frac{1}{\epsilon_{op}} - \frac{1}{\epsilon_S}\right)\left(\frac{1}{2a} - \frac{1}{4R_e}\right) \qquad (22)$$

where N_A is the Avogadro constant, Δe is the net charge transferred, and a is the effective radius of the reactant sphere.

A straightforward implementation of eq 22 predicts an increase in $\Delta G^*_{r(OS)}$ with an increase in the electrode−reactant separation distance (Figure 6, the middle curve). For the case of our redox system $a = 4.3$ Å (effective radius of reactant ions, $Fe(CN)_6^{3-/4-}$), and when the bare electrode is involved, $R_e = 4.3 + 3.6 = 7.9$ Å (where 3.6 Å stands for a diameter of specifically adsorbed Cl^- ion; see section 3 and the previous subsection for more detail). At this separation distance a value of $\epsilon_S = 20$ in eq 22 predicts that $\Delta G^*_{r(OS)} = 14.0$ kcal mol^{-1}. For the hypothetical case of close contact between the redox species and the bare electrode, eq 22 predicts a value of $\Delta G^*_{r(OS)} = 10.5$ kcal mol^{-1}.

A more sophisticated treatment of reorganization effects, developed by Liu and Newton,[14a] uses a three-zone model that specifically accounts for the role of alkanethiol spacers. The estimates of the reorganization using this model (viz. eq 17 of ref 14a) with values of $\epsilon_S^I = \infty$ (metal), $\epsilon_S^{II} = 2.25$ (SAM film), and $\epsilon_S^{III} = 78$ (substitution of the latter value by $\epsilon_S^{III} = 20$ for the diffuse part of the double layer, which now begins at the outer border of SAM films, does not change the numerical result significantly) are depicted in Figure 6, the lower curve. These two models give similar results. The values are very close at short separation distances and differ only by a few kilocalories in the asymptotic region.

An experimental value of $\Delta G^*_r \sim 23$ kcal mol^{-1} (corresponding to $G^*_{r(OS)} \sim 21.5$ kcal mol^{-1}) was extracted from the Tafel-like current−voltage curve,[13e] obtained for Au electrodes that were derivatized with a $-S-(CH_2)_{16}-OH$ monolayer ($R_e \approx 20$ Å). This value is in reasonable agreement with the theoretical value predicted by the model of Liu and Newton ($\Delta G^*_{r(OS)} \approx 17.5$ kcal mol^{-1}) and substantiates its predictive power. In the discussion below, the reorganization energy curves (Marcus' and/or Liu−Newton's) were rescaled to yield a value of $\Delta G^*_{r(OS)} \sim 21.5$ kcal mol^{-1} at $R \approx 20$ Å (Figure 6, the upper curve). The corresponding values at R_e are listed in Table 1. We note that a decrease of ca. 12% for the value of $\Delta G^*_{r(OS)}$ can be expected for the highest sugar concentrations, on the basis of eq 22 and the bulk value of ϵ_S (see ref 22b). However, it is reasonable to assume that this effect is negligible at the OHP for this system.

It becomes clear from the above analysis that the experimental value of $\Delta G^*_r = 8.0 \pm 1.0$ kcal mol^{-1} for the process at the bare electrode is at least 2 times smaller than the theoretical values predicted by the models of Liu−Newton and Marcus for an actual electrode−reactant separation distance of 7.9 Å. In previous theoretical work[10b] it was predicted that a low experimental reorganization free energy (compared to the expected Marcus value) could *result from a freezing out of the Marcus-like energy barrier by the solvent friction mechanism*. Some experimental evidence for this phenomenon was found previously.[10f] In the present work this effect is demonstrated more rigorously. It is important to realize that the lowering of the Marcus barrier discussed here is different from the lowering of the activation free energy by a large value of the electronic coupling matrix element (according to eq 13). The effect is evident in each of the free energies, ΔG^*_a and ΔG^*_r, at the same electrode−reactant separation distance of 7.9 Å (actual) or 4.3 Å (hypothetical); see Table 1. It should be noted that including

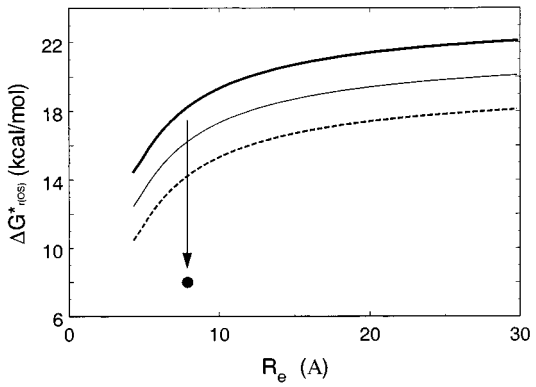

Figure 6. Curves showing the dependence of the outer-sphere reorganization free energy on the electrode−reactant distance: according to the model of Liu and Newton (dashed (bottom) curve), Marcus model (thin black (middle) curve), and the rescaled curve (thick black (top) curve). The arrow points to the experimental value for a bare electrode (filled circle).

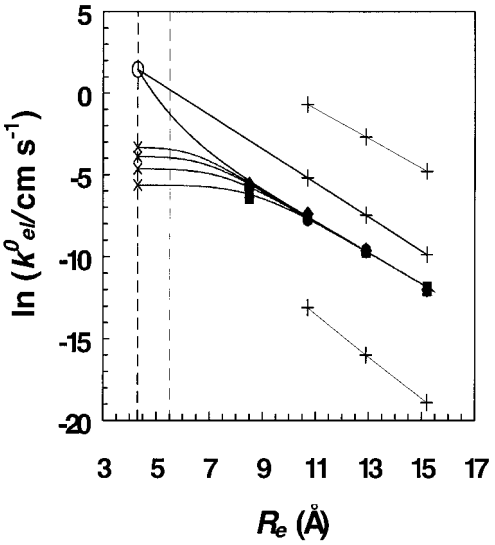

Figure 7. Data of Figure 3 plotted against the electrode−reactant separation distance (see Figure 3 caption). Simulated curves for the experimental (eq 23) and nonadiabatic rate constants are also drawn (see text for details).

the electric field penetration into the metal electrode and the spatial dispersion of the solution's dielectric response near the electrode surface does not account for the low value of the reorganization energy. The work of Kornyshev et al.[36] indicates that such effects may be small for larger reactant ions. For the $Fe(CN)_6^{3-/4-}$ redox couple a nearly constant value of $\Delta G^*_{r(OS)} \sim 20$ kcal mol^{-1}, almost independent of electrode−reactant separation distance, is expected. Thus, consideration of Kornyshev's model makes the lowering of the Marcus barrier appear more dramatic.

Electronic Coupling Matrix Element. The kinetic data obtained in the present work allows for a determination of the electronic coupling matrix element for the electron exchange processes at the bare Au electrode and the same electrode derivatized by SAMs of different thickness (i.e., at any electrode−reactant separation distance), provided that corrections for the distance-dependent variations of Φ and ΔG^*_r are incorporated. Figure 7 plots the data of Figure 2 (experimental points in filled symbols) against an actual electrode−reactant separation distance. The effective thickness of the *n*-alkanethiol chain lengths was determined from the results of ref 14a and a

reactant radius of 4.3 Å. The electronic coupling parameter (the magnitude of which determines the mechanism turnover) at different electrode−reactant separation distances was estimated from the rate constants obtained with SAM-coated electrodes at $n = 4$, 6, and 8, because they are viscosity independent and display the pure tunneling (nonadiabatic) mechanism. In Figure 7 the lower three points (crosses, thin line) correspond to these three experimental rate constants, corrected for the distance-dependent reactive site (the OHP) potential Φ_r by way of eqs 6, 7, and 20. The upper three points (crosses, thin line) represent the same rate constants that would be obtained for a distance independent reorganization free energy of $\Delta G_r^* = 15.9$ kcal mol^{-1}, but not correcting for the distance dependence of the potential Φ_r. The three points given by crosses situated above the experimental points and connected by a straight line that is extrapolated toward the smaller separation distances represent the rate constants that are corrected for the distance dependence of both the double-layer potential and the reorganization energy (but not for ΔG_a^*). It is clear that these two factors give corrections to the experimental data in opposite directions and almost compensate each other.

At some minimum distance the extrapolated line should correspond to the rate constant of a process proceeding at the bare electrode, but in the nonadiabatic regime.[5−8] When estimating values of the distance dependent solvent reorganization free energy, the charge-transfer distance for the bare electrode of $R_e = 7.9$ Å, which accounts for a layer of specifically adsorbed chloride ions, was used. In contrast, the Cl^- radius does not contribute to the electrode−reactant separation for the SAM-coated electrodes. Rather, the electrode−reactant separation distances are determined from the thickness of SAM layers and the reactant's radius, $a = 4.3$ Å. As a result, the extrapolated value for a separation distance should not "see" the adsorbed chloride, but the SAM thickness and the reactant's radius only. Thus, the extrapolated value of the rate constant should correspond to the rate constant for a hypothetical nonadiabatic process at the close contact of the reactant ion and the bare Au electrode (in virtual absence of the Cl^-), with $R_e = 4.3$ Å. Any comparison between the two hypothetical nonadiabatic mechanisms for the rate constants at separation distances of $R_e = 4.3$ Å and $R_e = 7.9$ Å should account for differences in the parameters $\Delta G_r^*(\Delta G_a^*)$ and H_{if} (see Table 1). It should be mentioned that any participation of the bridging ion, K^+, or of Cl^- in the superexchange mechanism has been excluded throughout the preceding discussion (see ref 32b for a more detailed analysis of the role of K^+). It was suggested earlier[37] that bridging ions may facilitate electron tunneling through the parameter H_{if} (vide infra), however, the off-resonance character of the electronic states of Cl^- and K^+ ions suggest that this pathway will not be significant for the SAM-coated electrodes. In either case, the analysis for the parameters ΔG_r^* and ΔG_a^* would remain unchanged.[37d,e]

The extrapolated value of the rate constant for nonadiabatic electron transfer at the bare electrode ($R_e = 4.3$ Å) is $k^0_{el(NA)} = 4.3$ cm s^{-1}. Equation 12 gives a value of $H_{if}^0 = 3.5$ kcal mol^{-1} for values of $\Delta G_r^* = 15.9$ kcal mol^{-1} (see above) and $\rho_m = 0.012$ kcal^{-1} mol (the latter value was calculated analogously to the value for Hg in the ref 10c). The extrapolated straight line represents the change of the parameter H_{if} with the electrode−reactant separation distance. The slope of the plot of $\ln(k^0_{el(NA)})$ vs R_e gives a value of $\beta = 1.04 \pm 0.05$ Å, which is in good agreement with theoretical estimates and most experimental values.[12−17] The calculated values of H_{if} at different electrode−reactant separation distances (at $n = 0$, 2, 4, 6, and 8) are presented in Table 1. The value of $H_{if} = 0.4$ kcal mol^{-1} calculated for the case of $n = 2$ is reasonably close to the value specified in previous work (>0.7 kcal mol^{-1}) for the onset of the solvent friction regime[10c,20a,b] and is consistent with the turnover between the strong and weak coupling limits. Thus, it is probable that the actual value of H_{if} at the bare electrode (at $R_e = 7.9$ Å) lies in the range 3.5 kcal mol^{-1} (H_{if}^0) > $H_{if} \geq 0.7$ kcal mol^{-1} (the value of $H_{if} \approx 1$ kcal mol^{-1} that was assumed to estimate the ΔG_r^* and ΔG_a^* values is consistent with this finding). This coupling strength is large enough to establish the solvent friction mechanism at the bare electrode, even in the presence of the compact layer of specifically adsorbed Cl^- ions. The coupling in this case may involve the Cl^- and K^+ ions in the superexchange mechanism.

Finally, the entire range of experimental data can be fit by using the unified expression[10d,f] for the rate constant,

$$\frac{1}{k_{el}^0} = \frac{1}{k_{el(SF)}^0} + \frac{1}{k_{el(NA)}^0} \qquad k_{el}^0 = \frac{k_{el(NA)}^0}{1 + k_{el(NA)}^0/k_{el(SF)}^0} \quad (23)$$

This expression transforms into either of the two extreme mechanisms and provides the effective rate constant in the intermediate region. The curved plots in Figure 7 represent fits of the experimental points by means of eq 23 and account for the distance-dependent intrinsic parameters of the nonadiabatic rate constant, $k^0_{el(NA)}$. The distance dependence of $k^0_{el(NA)}$ is represented by the thin line curved upward in Figure 7. As for $k^0_{el(SF)}$, the experimental values obtained at different viscosities on the bare electrode were directly used for this plot, since the ΔG_r^* and Φ_r corrections compensate each other and the rate constant is independent of H_{if} in the strong coupling regime. As discussed above, the electronic coupling through insulating SAM films and Cl^- ions at the bare electrode are essentially different. Indeed, if the Cl^- ions specifically adsorbed on the Au surface were as insulating as SAM films, then the "full" solvent friction regime would not be observable at the minimum separation distance of 7.9 Å for the bare electrode. To account for this change in the coupling, the experimental points for the friction-dependent rate constants can be formally considered as shifted into the zone of much shorter electrode−reactant separation distances (indicated in Figure 7 by the vertical dashed lines). The small crosses on the left edge of the simulated curves correspond to the hypothetical case of the strong coupling rate constant at the distance of direct contact between the electrode and the reactant. The left side of these curves displays a plateau that reflects the distance independent character of the rate constant in the strong coupling limit, see eqs 8−10. In agreement with this model, the plateau region's extent increases with the increase of solution viscosity. It should be mentioned that the experimental points for the intermediate regime, corresponding to the alkanethiol SAM with $n = 2$, fall on the simulated curves to an accuracy of 2−4% (Figure 7). This agreement provides additional justification that an electron exchange at the Au electrode coated by an ethanethiol monolayer ($n = 2$) occurs through the intermediate mechanism between the solvent friction and nonadiabatic regimes and is not a mixture of different mechanisms that arises from the system inhomogeneity (i.e., the SAM defects).[38]

6. Conclusion

These studies changed the strength of the electronic coupling between a Au electrode and a redox species by changing the thickness of a SAM monolayer film. Using this approach, it

was possible to follow the transition of the electron transfer mechanism from the strongly coupled, adiabatic, regime in which the solvent friction controls the dynamics to the weakly coupled, nonadiabatic, regime. This transition was demonstrated on both qualitative and quantitative levels. A detailed analysis of the system accounted for the permeability of the SAMS by Cl^- ions, incorporated the potential drop through the double-layer region, and included the change in the reorganization free energy with distance. It was found that the changes in the potential drop and the reorganization energy, which change dramatically when going from the bare to the thinnest SAMs, counteract each other, and largely compensate for the current system. This quantitative analysis also demonstrates the existence of a freezing out of the Marcus barrier in the solvent friction regime, as predicted theoretically. Finally, it was possible to determine the electronic coupling strength as a function of the distance from the electrode and show that it evolves from a value of ca. 1 kcal/mol for the "bare" electrode (in the presence of specifically adsorbed Cl^- ions), to a value of ca. 0.3 kcal/mol in the intermediate regime at 8.5 Å and lower values in the weak coupling regime of ca. 11 Å and larger.

Acknowledgment. D.E.Kh, T.D.D., and D.H.W. are grateful to the National Research Council, Office of International Affairs, for a financial support in the framework of Twinning Program Grant, 1999-2000. D.E.Kh. and L.D.Z. also kindly acknowledge the Collaborative Linkage Grant (PST.CLG 975701) from the North Atlantic Treaty Organization. D.H.W. acknowledges partial support from the Department of Energy, Division of Chemical Sciences (DE-FG02-89ER14062). We are grateful to Prof. L. I. Krishtalik for expert comments on the Kornyshev's model. We thank A. Napper for technical assistance and useful discussions.

References and Notes

(1) (a) Glasstone, S.; Laidler, K. J.; Eyring, H. *Theory of Rate Processes*; McGraw-Hill: New York, 1941. (b) Laidler, K. J. *Theories of Chemical Reaction Rates*; McGraw-Hill: New York, 1969.

(2) (a) Landau, L. D. *Phys. Z. Sowjet*. **1932**, *2*, 46. (b) Zener, C. *Proc. R. Soc. London A* **1932**, *137*, 696. (c) Landau, L. D.; Lifshits, E. M. *Quantum Mechanics, Nonrelativistic Theory*; Nauka: Moscow, 1974.

(3) (a) Marcus, R. A. *J. Chem. Phys*. **1956**, *24*, 966. (b) *J. Chem. Phys*. **1965**, *43*, 679. (c) *Annu. Rev. Phys. Chem*. **1964**, *15*, 155. (d) *J. Phys. Chem*. **1990**, *94*, 1050.

(4) (a) Hush, N. S. *J. Chem. Phys*. **1958**, *28*, 962. (b) *Trans. Faraday Soc*. **1961**, *57*, 557. (c) *Electrochim. Acta* **1968**, *13*, 1005.

(5) (a) Levich, V. G.; Dogonadze, R. R. *Dokl. Akad. Nauk SSSR* **1959**, *124*, 123. (b) Dogonadze, R. R.; Kuznetsov, A. M.; Vorotyntsev, M. A. *Phys. Status Solidi B* **1972**, *54*, 425. (c) Dogonadze, R. R.; Kuznetsov, A. M. *Prog. Surf. Sci*. **1975**, *6*, 1. (d) Kuznetsov, A. M. *Charge Transfer in Physics, Chemistry and Biology*; Gordon and Breach: Reading, MA, 1995.

(6) (a) Kestner, N. R.; Logan, J.; Jortner, J. *J. Phys. Chem*. **1974**, *78*, 2148. (b) Ulstrup, J.; Jortner, J. *J. Chem. Phys*. **1975**, *63*, 4358. (c) Ulstrup, J. *Charge-Transfer Processes in Condenced Media*; Springer: Berlin, 1979. (d) Bixon, M.; Jortner, J.; Michel-Beyrle, M. E. *Biochim. Biophys. Acta* **1991**, *1056*, 301.

(7) (a) Hopfield, J. J. *Proc. Natl. Acad. Sci. U.S.A.* **1974**, *71*, 3640. (b) Beratan, D. N.: Onuchic, J. N.; Hopfield J. J. *J. Chem. Phys*. **1987**, *86*, 4488. (c) Beratan, D. N.; Onuchic, J. N.; Winkler, J. R.; Gray, H. *Science* **1992**, *256*, 1007.

(8) (a) Sutin, N. *Prog. Inorg. Chem.* **1983**, *30* 441. (b) Newton, M. D.; Sutin, N. *Annu. Rev. Phys. Chem*. **1984**, *35*, 437. (c) Marcus, R. A.; Sutin, N. *Biochim. Biophys. Acta* **1985**, *811*, 265. (d) Newton, M. D. *Chem. Rev*. **1991**, *91*, 767.

(9) (a) Kramers, H. A. *Physica (Utrecht)* **1940**, *7*, 284. (b) Brinkman, H. C. *Physica (Utrecht)* **1956**, *12*, 149. (c) Landauer, R.; Swanson, J. A. *Phys. Rev*. **1961**, *121*, 1668.

(10) (a) Zusman, L. D. *Chem. Phys*. **1980**, *49*, 295. (b) *Chem. Phys*. **1983**, *80*, 29. (c) *Chem. Phys*. **1987**, *112*, 53. (d) *Chem. Phys*. **1988**, *119*, 51. (e) *Electrochim. Acta* **1991**, *36*, 395. (f) *Z. Phys. Chem*. **1994**, *186*, 1. (g) *J. Chem. Phys*. **1995**, *102*, 2580.

(11) (a) Alexandrov, I. V. *Chem. Phys*. **1980**, *51*, 449. (b) Calef, D. F.; Wolynes, P. G. *J. Phys. Chem*. **1983**, *87*, 3387. (c) Hynes, J. T. *J. Phys. Chem*. **1986**, *90*, 3701. (d) Heitele, H. *Angew. Chem., Int. Ed. Engl*. **1993**, *32*, 359. (e) Sumi, H. *Chem. Phys*. **1996**, *212*, 9.

(12) (a) Porter, M. D.; Bright, T. B.; Allara, D. L.; Chidsey, C. E. D. *J. Am. Chem. Soc.* **1987**, *109*, 3559. (b) Finklea, H. O.; Snider, D. A.; Fedyk, J.; Sabatani, E.; Gafni, Y.; Rubinstein, I. *Langmuir* **1993**, *9*, 3660. (c) Finklea, H. O. In *Electroanalytical Chemistry*; Bard, A. J., Rubinstein, I., Eds.; Marcel Dekker: New York, 1996; Vol. 19, p 109.

(13) (a) Miller, C.; Cuendet, P.; Grätzel, M. *J. Phys. Chem*. **1991**, *95*, 877. (b) Miller, C.; Grätzel, M. *J. Phys. Chem*. **1991**, *95*, 5225. (c) Becka, A. M.; Miller, C. *J. Phys. Chem*. **1992**, *96*, 2657. (d) Becka, A. M.; Miller, C. *J. Phys. Chem*. **1993**, *97*, 6233. (e) Terrettaz, S.; Becka, A. M.; Traub, M. J.; Fettinger, J. C.; Miller, C. J. *J. Phys. Chem*. **1995**, *99*, 11216.

(14) (a) Liu, Y.-P.; Newton, M. D. *J. Phys. Chem*. **1994**, *98*, 7162. (b) Smalley, J. F.; Feldberg, S. W.; Chidsey, C. E. D.; Linford, M. R.; Newton, M. D.; Liu, Y.-P. *J. Phys. Chem*. **1995**, *99*, 13141. (c) Guo, L.-H.; Facci, J. S.; McLendon, G. *J. Phys. Chem*. **1995**, *99*, 8458. (d) Curtiss, L. A.; Miller, J. R. *J. Phys. Chem. A* **1998**, *102*, 160.

(15) (a) Xu, J.; Li, H.-L.; Zhang, Y. *J. Phys. Chem*. **1993**, *97*, 11497. (b) French, M.; Creager, S. *Langmuir* **1998**, *14*, 2129. (c) Creager, S.; Yu, C. J.; Bamdad, C.; O'Connor, S.; MacLean, T.; Lam, E.; Chong, Y.; Olsen, G. T.; Luo, J.; Gozin; Kayyem, J. F. *J. Am. Chem. Soc*. **1999**, *121*, 1059. (d) Diao, P.; Jiang, D.; Cui, X.; Gu, D.; Tong, R.; Zhong, B. *J. Electroanal. Chem*. **1999**, *464*, 61.

(16) (a) Slowinski, K.; Chamberlain, R. V.; Bilewicz, R.; Majda, M. *J. Am. Chem. Soc*. **1996**, *118*, 4709. (b) Slowinski, K.; Chamberlain, R. V.; Miller, C. J.; Majda, M. *J. Am. Chem. Soc*. **1997**, *119*, 11910. (c) Slowinski, K.; Slowinska, K. U.; Majda, M. *J. Phys. Chem. B* **1999**, *103*, 8544.

(17) (a) Sheen, C. W.; Shi, J. X.; Martensson, J.; Parikh, A. N.; Allara, D. L. *J. Am. Chem. Soc*. **1992**, *114*, 1514. (b) Linford, M. R.; Chidsey, C. E. D. *J. Am. Chem. Soc*. **1993**, *115*, 12631. (c) Gu, Y.; Lin, Z.; Butera, R. A.; Smentkowski, V. S.; Waldeck, D. H. *Langmuir* **1995**, *11*, 1849. (d) Gu, Y.; Waldeck, D. H. *J. Phys. Chem*. **1996**, *100*, 9537. (e) Gu, Y.; Waldeck, D. H. *J. Phys. Chem. B* **1998**, *102*, 9015.

(18) (a) Kapturkievicz, A.; Behr, B. *J. Electroanal. Chem*. **1984**, *179*, 187. (b) Kapturkievicz, A.; Opallo, M. *J. Electroanal. Chem*. **1985**, *185*, 15. (c) Opallo, M.; Kapturkievicz, A. *Electrochim. Acta* **1985**, *30*, 1301. (d) Opallo, M. *J. Chem. Soc., Faraday Trans*. **1986**, *82*, 339.

(19) (a) Fawcett, W. R.; Foss, C. A. *J. Electroanal. Chem*. **1989**, *270*, 103. (b) Fawcett, W. R.; Foss, C. A. *J. Electroanal. Chem*. **1991**, *306*, 71. (c) Fawcett, W. R.; Foss, C. A. *Electrochim. Acta* **1991**, *36*, 1767. (d) Fawcett, W. R.; Opallo, M *J. Electroanal. Chem*. **1992**, *331*, 815.

(20) (a) Weaver, M. J.; Gennet, T. *Chem. Phys. Lett*. **1985**, *113*, 213. (b) Gennet, T.; Milner, D. F.; Weaver, M. J. *J. Phys. Chem*. **1985**, *89*, 2787. (c) McManis, G. E.; Golovin, M. N.; Weaver, M. J. *J. Phys. Chem*. **1986**, *90*, 6563. (d) Nielson, R. M.; Weaver, M. J. *J. Electroanal. Chem*. **1989**, *260*, 15. (e) Nielson, R. M.; McManis, G. E.; Weaver, M. J. *J. Phys. Chem*. **1989**, *93*, 4703. (f) Weaver, M. J.; Phelps, D. K.; Nielson, R. M.; Golovin, M. N.; McManis, G. E. *J. Phys. Chem*. **1990**, *94*, 2949.

(21) (a) Weaver, M. J.; McManis, G. E. *Acc. Chem. Res*. **1990**, *23*, 294. (b) Weaver, M. J. *Chem. Rev*. **1992**, *92*, 463. (c) Weaver, M. J. *J. Mol. Liqids* **1994**, *60*, 57. (d) Fawcett, W. R.; Opallo, M. *Angew. Chem., Int. Ed. Engl*. **1994**, *33*, 2131.

(22) (a) Zhang, X.; Leddy, J.; Bard, A. J. *J. Am. Chem. Soc*. **1985**, *107*, 3719. (b) Zhang, X.; Yang, H.; Bard, A. J. *J. Am. Chem. Soc*. **1987**, *109*, 1916. (c) Khoshtariya, D. E.; Dolidze, T. D.; Krulic, D.; Fatouros, N.; Devilliers, D. *J. Phys. Chem. B* **1998**, *102*, 7800.

(23) (a) Pyati, R.; Murray, R. W. *J. Am. Chem. Soc*. **1996**, *118*, 1743. (b) Williams, M. E.; Crooker, J. C.; Pyati, R.; Lyons, L. J.; Murray, R. W. *J. Am. Chem. Soc*. **1997**, *119*, 10249. (c) Fu, Y.; Cole, A. S.; Swaddle, T. W. *J. Am. Chem. Soc*. **1999**, *121*, 10410.

(24) (a) Goguadze, N. G.; Khoshtariya, D. E.; Hammerstad-Pedersen, J. M.; Ulstrup, J. *Eur. J. Biochem*. **1991**, *200*, 423. (b) Asano, T.; Furuta, H.; Sumi, H. *J. Am. Chem. Soc*. **1994**, *116*, 5545.

(25) (a) Daum, P. H.; Enke, C. G. *Anal. Chem*. **1969**, *41*, 653. (b) Kùta, J.; Yeager, E. *J. Electroanal. Chem*. **1975**, *59*, 110. (c) Peter, L. M.; Durrr, W.; Bindra, P.; Gerisher, H. *J. Electroanal. Chem*. **1976**, *71*, 31. (d) Mareèek, V.; Samec, Z.; Weber, J. *J. Electroanal. Chem*. **1978**, *94*, 169. (e) Dolidze, T. D.; Agladze, T. R. *Bull. Georgian Acad. Sci*. **1990**, *139*, 317. (f) Krulic, D.; Fatouros, N.; Khoshtariya, D. E. *J. Chim. Phys*. **1998**, *95*, 497.

(26) (a) Delahay, P. *Double Layer and Electrode Kinetics*; Interscience: New York, 1965. (b) Van Huong, C. N.; Clavilier, J. *Comput. Rend. C* **1971**, *272*, 1404. (c) Van Huong, C. N.; Clavilier, J.; Bonnemay, M. *J. Electroanal. Chem*. **1975**, *65*, 531.

(27) (a) Bard, A. J.; Faulkner, L. R. *Electrochemical Methods. Fundamentals and Application*; Wiley: New York, 1980; Chapter 6. (b) Bockris, J. O'M.; Reddy, A. K. N. *Modern Electrochemistry*; Plenum: New York, 1970; Vol. 2. (c) Roe, D. K. In *Laboratory Techiques in Electroanalytical Chemistry*; Kissinger, P. T., Heineman, W. R., Eds.; Marcel Dekker: New York, 1966; Chapter 7.

(28) (a) Nicholson, R. S. *Anal. Chem*. **1965**, *37*, 1351. (b) Greef, R.; Peat, R.; Peter L. M.; Pletcher D.; Robinson J. *Instrumental Methods in*

Electrochemistry. Southhampton Electrochemistry Group; Horwood: New York, 1986; Chapter 6.

(29) (a) Weaver, M. J. *Inorg. Chem*. **1979**, *18*, 402. (b) Tembe, B. L.; Friedman, H. L.; Newton, M. *J. Chem. Phys.* **1982**, *76*, 1490. (c) Hupp, J. T.; Weaver, M. J. *J. Electroanal. Chem.* **1983**, *152*, 1. (d) Newton, M. D.; Friedman, H. L. *J. Chem. Phys.* **1985**, *83*, 5210. (e) Gochev, A.; McManis, G. E.; Weaver, M. J. *J. Chem. Phys.* **1989**, *91*, 906.

(30) (a) Debye, P. *Polar Molecules*; Dover: New York, 1929. (b) Agmon, N. *J. Phys. Chem.* **1996**, *100*, 1072. (c) Fleming, G. R. *Chemical Applications of Ultrafast Spectroscopy*; Clarendon: Oxford, U.K., 1986. (d) Recent work (Buchner, R.; Barthel, J.; Gill, B. *Phys. Chem. Chem. Phys.* **1999**, *1*, 105) on aqueous solutions of La[Fe(CN)$_6$] shows that the relaxation time of water molecules does not change significantly upon the increase of electrolyte concentration. However, the contribution to the dielectric constant of the solution from the water, ϵ_s^W, decreases with increasing electrolyte concentration and may be extrapolated to a value as low as 20 for a 2 M solution. The effective value of $\epsilon_s \sim 20$ at the OHP is larger than the accepted value of $\epsilon_s \sim 10$ for the IHP (refs 26, 27, 33) and consistent with the proposition that this parameter changes smoothly when going to the OHP, and further to the bulk solution.

(31) (a) Riddick, J. A.; Bunger, W. B. *Techniques of Chemistry*; Wiley: New York, 1986; Vol. 3. (b) Khoshtariya, D. E.; Goguadze, N. G. *Russ. J. Phys. Chem*. **1987**, *61*, 1753. (c) Park, N. S.; Waldeck, D. H. *J. Phys. Chem.* **1990**, *94*, 662.

(32) (a) Khoshtariya, D. E.; Bajaj, H. C.; Tregloan, P. A.; Van Eldik, R. *J. Phys. Chem. A* **2000**, *104*, 5535. (b) Khoshtariya, D. E.; Dolidze, T. D.; Neubrand, A.; Van Eldik, R. *J. Mol. Liq.*, in press.

(33) (a) Graheme, D. C. *Annu. Rev. Phys. Chem*. **1955**, *6*, 337. (b) Conway, B. E. *Theory and Principles of Electrode Processes*; Ronald Press: New York, 1965; Chapters 4 and 5. (c) Bard A. J.; Faulkner L. R. *Electrochemical Methods. Fundamentals and Application*; Wiley: New York, 1980; Chapter12.

(34) The Gouy−Chapman−Stern model for the case of concentrated electrolyte solutions should only be used semiqualitatively. Our data evaluation (Table 1) is not based on this model and the corresponding estimates are provided for illustrative purposes only.

(35) The capacitance data (Figure 4) indicate that the Cl^- coverage starts to decrease slightly at $n = 6$ and is more pronounced at $n = 8$. However, for these larger n, the changes in Φ_r according to eq 20, are already small (Table 1), and the error arising from the corresponding deviations should be negligible.

(36) (a) Kornyshev, A. A *Electrochim. Acta* **1981**, *26*, 1. (b) Dzhavakhidze, P. G.; Kornyshev, A. A.; Krishtalik, L. I. *J. Electroanal. Chem*. **1987**, *228*, 329. (c) Phelps, D. K.; Kornyshev, A. A.; Weaver, M. J. *J. Phys. Chem*. **1990**, *94*, 1454.

(37) (a) Dogonadze, R. R.; Kharkats, Y. I.; Ulstrup, J. *J. Electroanal. Chem*. **1972**, *39*, 47. (b) *J. Electroanal. Chem*. **1973**, *43*, 161. (c) Zusman, L. D.; Beratan, D. N. *J. Chem. Phys*. **1997**, *105*, 165. (d) *J. Chem. Phys*. **1999**, *110*, 10468. (e) Iversen, G.; Friis, E. P.; Kharkats, Y. I.; Kuznetsov, A. M.; Ulstrup, J. *J. Biol. Inorg. Chem*. **1998**, *3*, 229.

(38) Because of the insulator character of SAM films, any kind of structural defects would lead to an increase of the heterogeneous standard rate constant compared to the case of the perfect coverage. This should be manifest by an upward deviation of the corresponding experimental points depicted in Figure 7. In fact, we observe either an excellent correspondence of these points with the simulated curves or a slight deviation in the opposite direction.